INTERNATIONAL JOURNAL FOR NUMERICAL METHODS IN FLUIDS
Int. J. Numer. Meth. Fluids 2013; **72**:724–747
Published online 26 Dec 2012 in Wiley Online Library (wileyonlinelibrary.com/journal/nmf). DOI: 10.1002/fld.3765

Implementation of slip boundary conditions in the finite volume method: new techniques

L. L. Ferrás[1,*,†], J. M. Nóbrega[1,‡] and F. T. Pinho[2,§]

[1]*Institute for Polymers and Composites/I3N, University of Minho, Campus de Azurém 4800-058 Guimarães, Portugal*
[2]*Centro de Estudos de Fenómenos de Transporte, Faculdade de Engenharia da Universidade do Porto, Rua Dr. Roberto Frias s/n, 4200-465 Porto, Portugal*

SUMMARY

Two different techniques for the implementation of the linear and nonlinear slip boundary conditions into a finite volume method based numerical code are presented. For the linear Navier slip boundary condition, an implicit implementation in the system of equations is carried out for which there is no need for any relaxation, especially when handling high slip coefficients. For three different nonlinear slip boundary conditions, two different methods are devised, one based on solving a transcendental equation for the boundary and the other on the linearization of the slip law. For assessment purposes, comparison is made between these new methods and the usual iterative process. With these new methods, the convergence difficulties, typical of the iterative procedure, are eliminated, and for some of the test cases, the convergence rate even increased with the slip velocity. The details of these implementations are given first for a simple geometry using orthogonal meshes and Cartesian coordinates followed by their generalization to non-Cartesian coordinates and nonorthogonal meshes. The developed code was tested in the benchmark slip-stick and 4:1 contraction flows, evidencing the robustness of the proposed procedures.

Received 25 January 2012; Revised 8 October 2012; Accepted 18 November 2012

KEY WORDS: slip boundary condition; finite volume method; implicit method

1. INTRODUCTION

Most of the literature related to the computation of the Navier–Stokes equations with slip boundary conditions is based on the finite element method (FEM). Some works present the variational and FEM studies of the Stokes and Navier–Stokes equations with free slip boundary conditions (see [1, 2] and the literature cited therein). Others give friction an important role and investigate the effects of slip and leak boundary conditions [3, 4].

This paper concerns friction slip models. Even though a number of difficulties have been reported in the FEM literature on handling friction slip models [3], some recent techniques, such as the penalty approach [4], seem to work well, at least when applied to Stokes flow. However, other contributions using linear and nonlinear slip models in the context of FEM [5–7] frequently refer the need to use relaxation in order to obtain convergence.

To our best knowledge, numerical codes based on the finite volume method (FVM) comprising slip boundary conditions are scarce, and a comparison between FEM and FVM shows that the solver for the Navier–Stokes equations is often quite different: whereas FEM is usually built in the variational formulation of the boundary value problem and iteratively couple the equations, on the basis

*Correspondence to: L. L. Ferrás, Institute for Polymers and Composites/I3N, University of Minho, Campus de Azurém 4800-058 Guimarães, Portugal.

†E-mail: luis.ferras@dep.uminho.pt

‡E-mail: mnobrega@dep.uminho.pt

§E-mail: fpinho@fe.up.pt

of projection [8], penalty or augmented-Lagrangian [4] methods, amongst others, the FVM uses the integral formulation of the Navier–Stokes equations together with one of the various SIMPLE-based [9] methods to develop and couple pressure and velocity fields along iterations [10]. Although the SIMPLE method is a disguised version of a projection method, results about the implementation of slip boundary conditions making use of FEM and projection methods could not be found in the literature, except for the case of an explicit implementation of slip boundary conditions. This makes it rather difficult to compare the implementation techniques of the slip models.

The aim of this paper is then to present a detailed description of two new different implementations of slip boundary conditions within an FVM approach. These methodologies do not need the use of relaxation and work well for all the slip boundary conditions. In addition, two other specific methods, one for the linear Navier slip law and the other for the nonlinear Navier slip law, are also presented.

The remainder of this paper is organized as follows. The next section presents the governing equations and is followed, in Section 3, by a detailed description of the implementation of slip velocity in a 2D flow using Cartesian coordinates. In Section 3, we first compare 'the classical' fully explicit method (which is applied to the four different slip boundary conditions, namely the linear and especially three nonlinear slip boundary conditions) with the fully implicit method for the linear Navier slip law, and then present two new different methods able to deal with all the slip laws studied here. The first of these two methods only works for orthogonal meshes, whereas the second method is able to handle both orthogonal and nonorthogonal meshes. The description of the four methods is followed by the presentation and discussion of results using reference cases for validation, prior to the closure of the paper.

2. GOVERNING EQUATIONS AND NUMERICAL METHOD

The governing equations for incompressible fluids are the continuity,

$$\nabla \cdot \mathbf{u} = 0 \tag{1}$$

and momentum equations,

$$\frac{\partial \rho \mathbf{u}}{\partial t} + \rho \nabla \cdot \mathbf{u}\mathbf{u} = -\nabla p + \nabla \cdot \boldsymbol{\tau} \tag{2}$$

where $\mathbf{u}$ is the velocity vector, ρ is the fluid density (assumed to be constant), p is the pressure and $\boldsymbol{\tau} = \boldsymbol{\tau}_s + \boldsymbol{\tau}_p$ is the extra stress tensor. The extra stress tensor is divided into solvent $\boldsymbol{\tau}_s = \eta_s(\nabla \mathbf{u} + (\nabla \mathbf{u})^T)$ (with η_s the solvent viscosity) and polymer $\boldsymbol{\tau}_p$ contributions, the latter given here by the following differential constitutive equation, called the simplified Phan-Thien–Tanner model (sPTT) [11, 12]:

$$f(tr\boldsymbol{\tau}_p)\boldsymbol{\tau}_p + \lambda\left(\frac{\partial \boldsymbol{\tau}_p}{\partial t} + \mathbf{u}.\nabla\boldsymbol{\tau}_p - \left[(\nabla \mathbf{u})^T.\boldsymbol{\tau}_p + \boldsymbol{\tau}_p.\nabla\mathbf{u}\right]\right) = \eta_p(\nabla\mathbf{u} + (\nabla\mathbf{u})^T) \tag{3}$$

where $f(tr\boldsymbol{\tau}_p)$ is a function depending on the trace (tr) of the polymeric stress tensor $(\boldsymbol{\tau}_p)$, λ is the relaxation time and η_p is the zero shear polymer viscosity. In the literature, there are two possible functions for $f(tr\boldsymbol{\tau}_p)$. The original linear function, presented by Phan-Thien and Tanner[11],

$$f(tr\boldsymbol{\tau}_p) = 1 + \frac{\varepsilon\lambda}{\eta_p} tr[\boldsymbol{\tau}_p] \tag{4}$$

and the exponential proposed later by Phan-Thien [12], which is given by

$$f(tr\boldsymbol{\tau}_p) = \exp\left(\frac{\varepsilon\lambda}{\eta_p} tr[\boldsymbol{\tau}_p]\right) \tag{5}$$

In any case, the parameter ε is related to the elongational behavior of the modeled fluid (ε is inversely proportional to the extensional viscosity).

DOI: 10.1002/fld

The Upper-convected Maxwell (UCM) model can be derived from the sPTT model by making $\eta_s = \varepsilon = 0$, and the Oldroyd-B model is obtained when $\varepsilon = 0$ and $\eta_s \neq 0$. The generalized-Newtonian fluid model assumes $\boldsymbol{\tau} = \boldsymbol{\tau}_s + \boldsymbol{\tau}_p = 2\eta(\dot{\gamma})\boldsymbol{S}$ in Equation (2), where $\eta(\dot{\gamma})$ is a viscosity function that depends on the second invariant ($\dot{\gamma}$) of the rate of deformation tensor $\boldsymbol{S} = \left(\nabla\mathbf{u} + (\nabla\mathbf{u})^T\right)/2$ with $\dot{\gamma} = \sqrt{2\boldsymbol{S} : \boldsymbol{S}}$).

A fully implicit finite volume numerical method is used to solve Equations (1)–(3), which are transformed to generalized coordinates. The method is based on a time marching pressure-correction algorithm formulated with a collocated variable arrangement. The governing equations are integrated in space over the control volumes (cells with volume V_P) forming the computational mesh and in time over a time step (Δt). The volume integration benefits from Gauss theorem, and the subsequent surface integrals are then discretized with the help of the midpoint rule so that sets of linearized algebraic equations are obtained, having the following general form:

$$a_{\mathrm{P}}\mathbf{u}_{\mathrm{P}} = \sum_{\mathrm{F}=1}^{6} a_{\mathrm{F}}\mathbf{u}_{\mathrm{F}} + S_{\mathbf{u}} \tag{6}$$

for the velocity components u, v and w, and

$$a^{\tau}_{\mathrm{P}}\boldsymbol{\tau}_{\mathrm{P}} = \sum_{\mathrm{F}=1}^{6} a^{\tau}_{\mathrm{F}}\boldsymbol{\tau}_{\mathrm{F}} + S_{\boldsymbol{\tau}} \tag{7}$$

for the extra stress components τ_{xx}, τ_{xy}, τ_{xz}, τ_{yz}, τ_{yy} and τ_{zz}. In these equations, a_{P}, a_{F}, a^{τ}_{P} and a^{τ}_{F} are the coefficients accounting for convection and diffusion influences, $S_{\mathbf{u}}$ and $S_{\boldsymbol{\tau}}$ are source terms encompassing all contributions not included in the coefficients, the subscript P denotes the cell under consideration and subscript F its corresponding neighboring cells. The central coefficients of the discretized equations, a_{P} and a^{τ}_{P}, are generally given by the sum of neighbor cell coefficients in addition to the time-dependent term in the corresponding governing equation (the time is used here with the purpose of inertial under-relaxation because the interest is only in steady state solutions). As follows, the central coefficient for the momentum equation is given by

$$a_{\mathrm{P}} = \frac{\rho V_{\mathrm{P}}}{\Delta t} + \sum_{\mathrm{F}=1}^{6} a_{\mathrm{F}} \tag{8}$$

but for the sPTT stress equations, an additional term is included, resulting from the $f(tr\boldsymbol{\tau})$ term in Equation (3), which tends to promote stability by increasing the numerical value of the a_{P} coefficient,

$$a^{\tau}_{\mathrm{P}} = \frac{\lambda V_{\mathrm{P}}}{\Delta t} + V_{\mathrm{P}}\left(1 + \frac{\varepsilon\lambda}{\eta_{\mathrm{P}}} tr[\boldsymbol{\tau}_p]\right) + \sum_{\mathrm{F}=1}^{6} a^{\tau}_{\mathrm{F}} \tag{9}$$

The linear set of equations given by Equation (6) are sequentially solved for the Cartesian velocity components by means of a preconditioned biconjugate gradient solver (the preconditioner used is LDU decomposition special for indirect addressing). The newly computed velocity field usually does not satisfy the continuity equation (i.e., Equation (1)), which needs to be corrected by an adjustment of the pressure differences that drive them. This is accomplished by means of a pressure-correction field obtained from a discrete Poisson equation, derived from a discretized form of the continuity equation (Equation (1)) in combination with the momentum equation (Equation (2)). This pressure-correction equation is then solved by a symmetric conjugate gradient method. The correction of the velocity field follows the SIMPLEC strategy of Van Doormal and Raithby [13], and we may now solve sequentially the implicitly discretized constitutive equations for τ_{xx}, τ_{xy}, τ_{xz}, τ_{yz}, τ_{yy} and τ_{zz} (Equation (7)). This system of equations is solved with the help of the biconjugate gradient method.

Most important from the standpoint of accuracy is the representation of the convective terms in the constitutive equations, which relies on the SMART scheme of Gaskell and Lau [14]. A schematic view of the numerical procedure can be seen in Figure 1, and a detailed description of the code can be found in [10].

DOI: 10.1002/fld

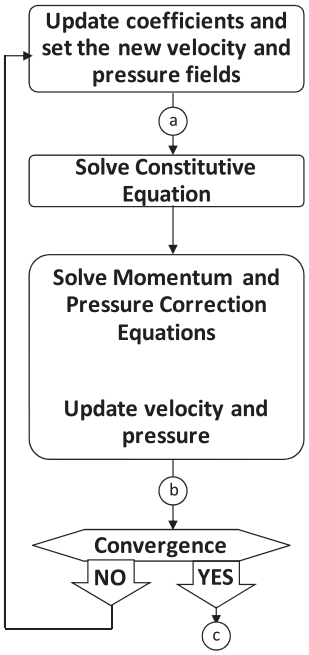

Figure 1. Schematic of the numerical procedure.

2.1. Boundary conditions

The slip boundary conditions used in this work are the linear [15] and nonlinear [16] Navier slip laws as well as the Hatzikiriakos [17] and asymptotic [18] slip laws, which are presented next.

Let $\mathbf{u}_t$ and $\boldsymbol{\tau}_t$ be the velocity and stress tangent (to the wall) vectors, respectively. It is required that the absolute value of the slip velocity must be a function of the absolute value of the tangent stress vector as in Equation (10),

$$\|\mathbf{u}_t\| = \|f(\boldsymbol{\tau}_t)\| \tag{10}$$

where $\|.\|$ stands for the usual l^2 norm and $f(.)$ represents any real linear or nonlinear function of the tangent stress vector ($\boldsymbol{\tau}_t$). It is also required that the tangent velocity vector, $\mathbf{u}_t$, should point in the opposite direction to the tangent stress vector $\boldsymbol{\tau}_t$, that is, the relationship between these two quantities is given by

$$\mathbf{u}_t = -\|f(\boldsymbol{\tau}_t)\| \, \|\boldsymbol{\tau}_t\|^{-1} \boldsymbol{\tau}_t \tag{11}$$

where the function$\|f(\boldsymbol{\tau}_t)\|$ takes the form in Equation (12) for each of the various slip laws

$$\|f(\boldsymbol{\tau}_t)\| = \begin{cases} \text{linear Navier} & k_l \|\boldsymbol{\tau}_t\| & \text{(a)} \\ \text{nonlinear Navier} & k_{nl} \|\boldsymbol{\tau}_t\|^m & \text{(b)} \\ \text{Hatzikiriakos} & k_{H1} \sinh(k_{H2} \|\boldsymbol{\tau}_t\|) & \text{(c)} \\ \text{asymptotic} & k_{A1} \ln(1 + k_{A2} \|\boldsymbol{\tau}_t\|) & \text{(d)} \end{cases} \tag{12}$$

and the parameters k_l, k_{nl}, k_{H1}, k_{H2}, k_{A1}, k_{A2} and m are the corresponding slip coefficients. The interested reader is referred to [19] for more details about these models.

3. NUMERICAL IMPLEMENTATION OF SLIP BOUNDARY CONDITIONS

3.1. Discretization

To better understand the implementation of slip boundary conditions, a simple 2D channel flow with Cartesian coordinates and orthogonal meshes is used, as illustrated in Figure 2. At the boundary

DOI: 10.1002/fld

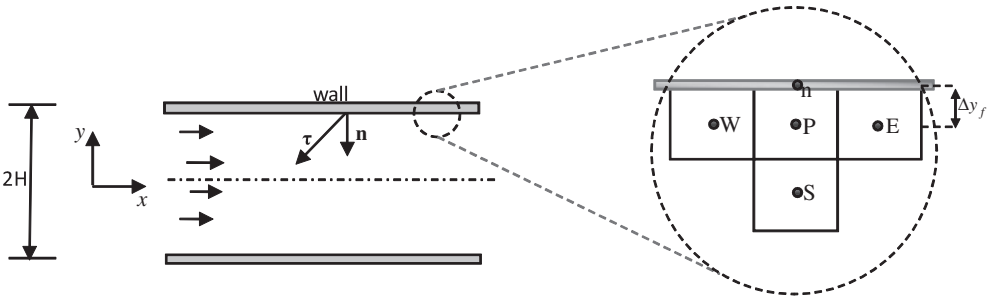

Figure 2. Simple geometry: flow between parallel plates (zoomed view of the computational cells near the wall).

(the wall at the north cell face), the velocity is tangent to the wall (x-direction), and the tangent stress vector is determined as

$$\boldsymbol{\tau}_t = (\mathbf{1} - \mathbf{n} \otimes \mathbf{n}^T)(\boldsymbol{\tau}\mathbf{n}^T) \tag{13}$$

where $\mathbf{n} = (n_1, n_2, n_3)$ is the normal vector to the wall and $\mathbf{1}$ is the identity matrix.

The main key for this new implementation of slip boundary conditions is the local assumption of a Couette flow in the vicinity of the wall [10]. If so, the tangent stress vector at the upper wall (for this simple geometry) can be written as

$$\boldsymbol{\tau}_t = \left(\mu(\dot{\gamma})\frac{\mathrm{d}u}{\mathrm{d}y}\right)_{\text{wall}} \tag{14}$$

for all the constitutive equations studied here.

On the basis of this, what distinguishes one viscoelastic model from another (with respect to the wall boundary treatment) is only the viscosity function $\mu(\dot{\gamma})_{\text{wall}}$, which is given by $\mu(\dot{\gamma})_{\text{wall}} \equiv \eta(\dot{\gamma}_{\text{wall}})$ for the generalized Newtonian fluids and is given by $\mu(\dot{\gamma})_{\text{wall}} \equiv \eta_s + \frac{\eta_p}{1+(\alpha-1)^2/3\alpha}$ (with $\alpha \equiv \left(\theta + \sqrt{\theta^2-1}\right)^{1/3}$ and $\theta \equiv 1+27\varepsilon(\lambda\dot{\gamma})^2_{\text{wall}}$) [20] for the PTT model.

Under these flow conditions, the slip law takes the form

$$u_{ws} = k_{nl}\left(-\mu(\dot{\gamma})\frac{du}{dy}\right)^m_{\text{wall}} \tag{15}$$

for the nonlinear Navier slip law. The linear law is recovered for $m = 1$ in which case $k_{nl} \equiv k_l$. The Hatzikiriakos and asymptotic slip laws are given by Equations (16) and (17), respectively.

$$u_{ws} = k_{H1}\sinh\left(-k_{H2}\mu(\dot{\gamma})\frac{\mathrm{d}u}{\mathrm{d}y}\right)_{\text{wall}} \tag{16}$$

$$u_{ws} = k_{A1}\ln\left(1 - k_{A2}\mu(\dot{\gamma})\frac{\mathrm{d}u}{\mathrm{d}y}\right)_{\text{wall}} \tag{17}$$

If we assume a one-sided first-order approximation for the derivative $\frac{\mathrm{d}u}{\mathrm{d}y}$ at the wall appearing in Equations (15)–(17), then $\frac{\mathrm{d}u}{\mathrm{d}y} \simeq \frac{u_{ws}-u_{\mathrm{P}}}{\Delta y_f}$, where ws stands for 'wall slip', u_{P} is the velocity at the center of the control volume adjacent to the wall and Δy_f is half the cell width, as shown in Figure 2. On the basis of this, Equations (15)–(17) can be written in their discretized form as functions of the difference $u_{ws} - u_P$,

$$u_{ws} = f_d(u_{ws} - u_{\mathrm{P}}) \equiv \begin{cases} \text{Navier} & k_{nl}\left(-\frac{\mu(\dot{\gamma})}{\Delta y_f}(u_{ws} - u_{\mathrm{P}})\right)^m \quad \text{(a)} \\ \text{Hatzikiriakos} & k_{H1}\sinh\left(-\frac{k_{H2}\mu(\dot{\gamma})}{\Delta y_f}(u_{ws} - \mathrm{u_P})\right) \quad \text{(b)} \\ \text{asymptotic} & k_{A1}\ln\left(1 - \frac{k_{A2}\mu(\dot{\gamma})}{\Delta y_f}(u_{ws} - u_{\mathrm{P}})\right) \quad \text{(c)} \end{cases} \tag{18}$$

DOI: 10.1002/fld

where $f_d(\,)$ represents the discretized version of the slip laws.

The discretization of the continuity equation (Equation (1)) in a computational cell P (Figure 2) results in the balance of mass fluxes for this cell. These fluxes are normal to the cell faces; therefore, the slip boundary condition has no direct influence on this equation, because the walls are impermeable.

The momentum equation (Equation (2)) is directly affected by the slip boundary condition through the term $\nabla\cdot\boldsymbol{\tau}$. Notice that the discretization of this term will also change with the assumption of a Couette flow in the vicinity of the wall (Equation (14)) as shown in Appendix A.

3.2. Explicit and implicit implementations of the Navier slip law

3.2.1. Explicit formulation. For the implementation of the slip boundary conditions with an explicit slip formulation, a SIMPLE-type [9] method is used as an example. It can be easily adapted to other algorithms such as the SIMPLEC, SIMPLER or PISO.

Let i represent the number of the outer iteration (iteration between the linearized momentum equation and the pressure-correction equation), then the discretized slip boundary condition at iteration i is given for the linear Navier slip law by

$$u_{ws}^{i} = k_l \left(-\mu(\dot{\gamma})_{\text{wall}}^{i-1} \frac{u_{ws}^{i-1} - u_{\text{P}}^{i-1}}{\Delta y_f} \right) \tag{19}$$

where $\mu(\dot{\gamma})_{\text{wall}}^{i-1}$, u_{ws}^{i-1}, u_{P}^{i-1} pertain to the previous iteration.

The proposed modified SIMPLE algorithm (SIMPLE-SLIP-Explicit (SSE)) is given in Figure 1 with the following additional step:

(a) Compute slip velocity with the discretized slip model given by Equation (19).

This slip velocity value u_{ws}^{i} goes straight to the source term $S_{\mathbf{u}}$ of Equation (6) (see Appendix A for more details).

At each iteration i, the boundary condition is updated with the velocity from the previous iteration $i-1$. To achieve convergence, the variation of this boundary condition along the iterative process must be stable in some sense (sudden changes in the boundary condition along the iterative process will not allow the overall convergence, and for a well-posed problem, we want the flow to depend continuously on the boundary data).

The example illustrated in Figure 3 shows a case where convergence is not achieved for a situation where the linear Navier slip boundary condition was employed. There, we can see the evolution of the velocity at the center of a control volume with the north face coinciding with a wall, as in

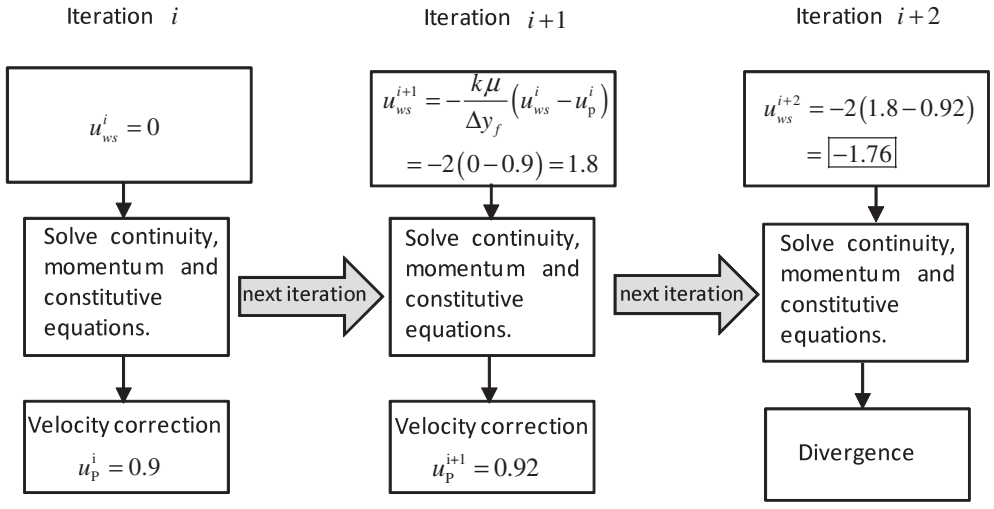

Figure 3. Example of the iterative procedure used for the explicit formulation of slip velocity.

DOI: 10.1002/fld

Figure 2. The fluid movement is from left to right (with imposed velocity of 1 m/s), but at iteration $i+2$, the calculations are made assuming the fluid is slipping at the wall from the right to the left, whereas just next to the wall, the fluid flows in the opposite direction. Because of this inconsistency, non-physical characteristics appear, and the process either diverges or converges to an unacceptable solution.

The relationship $u_{ws} < u_{\mathrm{P}}$ seems to be the key to the convergence of the process, but this is difficult to guarantee when calculating the slip velocity with the values from the previous iteration. A possible remedy is the classical use of under-relaxation $u^i_{ws} = Ru^{i-1}_{ws} + (1-R)u^i_{ws}$ with $R < 1$ when updating the slip velocity in step (a) (Flowchart illustrated in Figure 1), but for high slip coefficients and nonlinear slip laws, this does not work.

Remark: This method can also be applied to any of the other slip laws studied here, provided the right-hand side of Equation (19) is evaluated with the values from the previous iteration, $i-1$, by $u^i_{ws} = f_d(u^{i-1}_{ws} - u^{i-1}_{\mathrm{P}})$.

3.2.2. Implicit formulation. To eliminate the convergence issues of the explicit method, a fully implicit formulation can be implemented, but only the linear Navier slip law allows a fully implicit method without the use of other techniques (such as a deferred correction). The idea is to evaluate Equation (19) assuming all variables come from the present iteration. Equation (19) can then be rewritten as

$$u^i_{ws} = k_l\left(-\mu(\dot{\gamma})^i_{\mathrm{wall}}\frac{(u^i_{ws}-u^i_{\mathrm{P}})}{\Delta y_f}\right) \Leftrightarrow u^i_{ws} = \frac{a}{a+1}u^i_{\mathrm{P}} \text{ with } a=k_l\left(-\frac{\mu(\dot{\gamma})^i_{\mathrm{wall}}}{\Delta y_f}\right) \tag{20}$$

This ensures that the slip velocity is always smaller than the velocity at the center of the adjacent computational cell, so the continuity/monotonicity we searched for is preserved.

The dependency of u^i_{ws} on u^i_{P} leads to modifications in Equations (6) and (8) with the central coefficient a_{P} (Equation (8)) now being given by

$$a_{\mathrm{P}} = a_{\mathrm{E}} + a_{\mathrm{W}} + a_{\mathrm{S}} + \frac{a_{\mathrm{N}}}{a+1} + \frac{\Delta V_{\mathrm{P}}\rho^0_{\mathrm{P}}}{\Delta t} \tag{21}$$

These equations differ from those for no slip velocity (Equations (6) and (8)), in that the term $a_{\mathrm{N}}u_{\mathrm{N}}$ in Equation (6) does not exist and the coefficient a_{N} in Equation (8) is now multiplied by $\frac{1}{a+1}$; therefore, in Equation (21), a_{P} is smaller when compared with the a_{P} of Equation (8). Even though this implicit implementation brings a less diagonally dominant system of equations, the required conditions for convergence and stability are maintained, such as $a_{\mathrm{P}} \geqslant \sum a_{\mathrm{F}}$.

With this implicit implementation, there is no need to specify the value of u_{ws} along the iterative process and no need to use under-relaxation to solve the discrete system of equations that results from the discretization of the momentum equation. When convergence is achieved, the slip velocity can be calculated with Equation (20) at each of the wall computational cells.

The iterative procedure, here called SIMPLE-SLIP-Implicit (SSI) scheme, is given by the scheme of Figure 1 with the following additional step:

(c) After convergence, compute the slip velocity with the discretized slip model $u^i_{ws} = \frac{a}{a+1}u^i_{\mathrm{P}}$, for all boundary wall computational cells.

Notice that $\lim(\Delta y_f \to 0)\frac{1}{a+1} = 0$, and this means that the refinement of the mesh near the wall does not improve the convergence of the iterative matrix solver.

For a formulation with a second-order approximation of the derivative $\frac{\mathrm{d}u}{\mathrm{d}y}_{\mathrm{wall}}$ (derivative of the slip law), see Appendix B.

3.3. Semi-implicit implementation of slip laws (orthogonal meshes)

As mentioned before, the fully implicit formulation can only by applied to the linear Navier slip law. To implement the other slip laws implicitly, we devised the method described in the following text.

DOI: 10.1002/fld

Consider again the geometry of Figure 2. The idea behind this new method is to assume the slip velocity implicit on both sides of the equation for each of the wall boundary cells at each iteration i,

$$u_{ws}^{i} = f_d(u_{ws}^{i} - u_{\mathrm{P}}^{i-1}) \tag{22}$$

and then use a numerical scheme to find the roots of the ensuing transcendent equation. It can be proved analytically that with this method, $u_{ws}^{i} < u_{\mathrm{P}}^{i-1}$ for all the slip boundary conditions studied here (Appendix C). In particular, we have the bounds $[a;\, b]$ for the solution u_{ws}^{i} that are given by Equations (23), (24) and (25) for the nonlinear Navier, Hatzikiriakos and asymptotic slip laws, respectively:

$$[a;\, b] \equiv [0;\, u_{\mathrm{P}}^{i-1}] \tag{23}$$

$$[a;\, b] \equiv \left[\frac{k_{H1}k_{H2}\mu(\dot{\gamma})_{\mathrm{wall}}^{i-1}/\Delta y_f}{k_{H1}k_{H2}\mu(\dot{\gamma})_{\mathrm{wall}}^{i-1}/\Delta y_f + 1};\, u_{\mathrm{P}}^{i-1}\right] \tag{24}$$

$$[a;\, b] \equiv \begin{cases} [0;\, u_{\mathrm{P}}^{i-1}] & \text{if } k_{A1} \geqslant 1 \\ \left[0;\, \frac{k_{A1}k_{A2}\mu(\dot{\gamma})_{\mathrm{wall}}^{i-1} + k_{A1}\Delta y_f}{k_{A1}k_{A2}\mu(\dot{\gamma})_{\mathrm{wall}}^{i-1} + \Delta y_f} u_{\mathrm{P}}^{i-1}\right] & \text{if } k_{A1} < 1 \end{cases} \tag{25}$$

Here, the bisection method was used to find the roots of the transcendent equation (Equation (22)), starting in the range of Equations (23)–(25) and stopping after n iterations such that $(b-a)/2^n$ is below a given error.

The canonical equation used to compute the velocity field is still Equation (6) with the central coefficient given by Equation (8).

With this method, the new iterative algorithm (SIMPLE-SLIP-Semi-Implicit-transcendent (SSSIT)) follows the SIMPLE scheme, shown in Figure 1, with the following additional step:

(a) Compute slip velocity with the discretized slip model $u_{ws}^{i} = f_d(u_{ws}^{i} - u_{\mathrm{P}}^{i-1})$ by applying the bisection method.

3.4. Semi-implicit implementation of slip laws (orthogonal and nonorthogonal meshes)

The SSSIT algorithm solves the convergence problems for linear and nonlinear slip laws but only works for orthogonal meshes. A new semi-implicit method is now devised, which is able to deal with both orthogonal and nonorthogonal meshes, which is inspired on the linearization used with the Navier slip law (fully implicit formulation).

The slip velocity u_{ws} can usually be written as a function of the difference $(u_{ws} - u_{\mathrm{P}})$ by $u_{ws} = f_d(u_{ws} - u_{\mathrm{P}})$. If we multiply this function by the ratio $\frac{u_{ws}-u_{\mathrm{P}}}{|u_{ws}-u_{\mathrm{P}}|}$, then our slip law can be rewritten as

$$u_{ws} = f_d(u_{ws} - u_{\mathrm{P}})\frac{u_{ws} - u_{\mathrm{P}}}{|u_{ws} - u_{\mathrm{P}}|} \tag{26}$$

and, if along the iterative procedure only the slip velocity in the numerator is taken from the present iteration $\frac{u_{ws}^{i}-u_{\mathrm{P}}^{i-1}}{|u_{ws}^{i-1}-u_{\mathrm{P}}^{i-1}|}$, then the general slip boundary condition becomes

$$u_{ws}^{i} = \frac{c}{c+1}u_{\mathrm{P}}^{i-1} \tag{27}$$

with $c = f_d(u_{ws}^{i-1} - u_{\mathrm{P}}^{i-1})/|u_{ws}^{i-1} - u_{\mathrm{P}}^{i-1}|$. Because $\frac{c}{c+1} < 1$, we guarantee once again the continuity/monotonicity of the slip velocity. The specification of c for each of the slip laws studied here is straightforward.

Notice that although $\left\|(u_{ws}^{i} - u_{\mathrm{P}}^{i})/|u_{ws}^{i} - u_{\mathrm{P}}^{i}|\right\| = 1$, along the calculations $\left\|(u_{ws}^{i} - u_{\mathrm{P}}^{i-1})/|u_{ws}^{i-1} - u_{\mathrm{P}}^{i-1}|\right\| \neq 1$. This ratio should tend to 1 as convergence is approached or else the slip velocity vector will not be pointing on the correct direction. This is another criterion that should be checked for convergence.

DOI: 10.1002/fld

The canonical equation used to compute the velocity field is again Equation (6) with the central coefficient given by Equation (8), and the iterative procedure (SIMPLE-SLIP-Semi-Implicit (SSSI)) follows the SIMPLE scheme, shown in Figure 1, with the following additional two steps:

(a) Compute slip velocity with the discretized slip model of Equation (27).
(b) Check for convergence in the residuals of the system of equations and for $\|(u_{ws}^{i} - u_{\mathrm{P}}^{i-1})/|u_{ws}^{i-1} - u_{\mathrm{P}}^{i-1}|\| \to 1$. If convergence is not achieved, then proceed to the beginning of the iteration. (The nonlinear Navier slip law can be treated as a special case of this method. For more details, see Appendix D.)

The generalization to nonorthogonal meshes is straightforward but takes some more work. Let $\boldsymbol{u}_t = (u_{1t}, u_{2t}, u_{3t})$ and $\boldsymbol{\tau}_t = (\boldsymbol{\tau}_{1t}, \boldsymbol{\tau}_{2t}, \boldsymbol{\tau}_{3t})$ be respectively the tangent (to the wall) velocity and stress vectors, both with Cartesian components. By Equation (11) and assuming Couette flow near the wall, we obtain the following general formula for all slip laws:

$$\mathbf{u}_{ws} = \pm f\left(\left\|\left(\mu(\dot{\gamma})\frac{\mathrm{d}\mathbf{u}}{\mathrm{d}\mathbf{n}}\right)_{\mathrm{wall}}\right\|\right)\frac{\left(\mu(\dot{\gamma})\frac{\mathrm{d}\mathbf{u}}{\mathrm{d}\mathbf{n}}\right)_{\mathrm{wall}}}{\left\|\left(\mu(\dot{\gamma})\frac{\mathrm{d}\mathbf{u}}{\mathrm{d}\mathbf{n}}\right)\right\|_{\mathrm{wall}}}, \tag{28}$$

where the $\pm$ depends on the sign of $\frac{\mathrm{d}\mathbf{u}}{\mathrm{d}\mathbf{n}}$, and $\frac{\mathrm{d}\mathbf{u}}{\mathrm{d}\mathbf{n}} = \left(\frac{\mathrm{d}u_{1t}}{\mathrm{d}\mathbf{n}}; \frac{\mathrm{d}u_{2t}}{\mathrm{d}\mathbf{n}}; \frac{\mathrm{d}u_{3t}}{\mathrm{d}\mathbf{n}}\right)$ with u_{jt}, $j = 1, 2, 3$, the components of the tangent vector at the wall.

The discretization of these derivatives is given by

$$\left(\frac{u_{1t} - u_{1t\mathrm{P}}}{\delta n}; \frac{u_{2t} - u_{2t\mathrm{P}}}{\delta n}; \frac{u_{3t} - u_{3t\mathrm{P}}}{\delta n}\right) \tag{29}$$

where δn is the distance between the wall and P′ (as given in Figure 4) and $u_{jt\mathrm{P}} = u_{j\mathrm{P}} - n_j \mathbf{u}.\mathbf{n}$, $j = 1, 2, 3$, are the components of the tangent velocity vector at the center of the adjacent cell P.

The velocity at P′ is not known (Figure 4), so it is assumed that $\mathbf{u}_{\mathrm{P}} = \mathbf{u}_{\mathrm{P}'}$. This introduces an error in the calculations that will diminish as the mesh quality and refinement are improved.

Considering that $\mu(\dot{\gamma})_{\mathrm{wall}}$ is a positive scalar and that only the slip velocity on the last term of Equation (28) is evaluated implicitly, then Equation (28) can be rewritten as

$$(u_1, u_2, u_3)_{ws}^{i} = \frac{d}{d+1}(u_{1t\mathrm{P}}; u_{2t\mathrm{P}}; u_{3t\mathrm{P}})^{i-1} \tag{30}$$

with

$$d \equiv \begin{cases} \text{Navier} & k_{nl}\,\|g\|^{m-1}\,(\mu(\dot{\gamma})_{\mathrm{wall}}^{i-1})^{m}/\delta n \quad \text{(a)} \\ \text{Hatzikiriakos} & k_{H1}\sinh(k_{H2}\left\|\mu(\dot{\gamma})_{\mathrm{wall}}^{i-1} g\right\|)\mu(\dot{\gamma})_{\mathrm{wall}}^{i-1}/\left\|\mu(\dot{\gamma})_{\mathrm{wall}}^{i-1} g\right\|\delta n \quad \text{(b)} \\ \text{asymptotic} & k_{A1}\ln(1 + k_{A2}\left\|\mu(\dot{\gamma})_{\mathrm{wall}}^{i-1} g\right\|)\mu(\dot{\gamma})_{\mathrm{wall}}^{i-1}/\left\|\mu(\dot{\gamma})_{\mathrm{wall}}^{i-1} g\right\|\delta n \quad \text{(c)} \end{cases} \tag{31}$$

and $g = (u_{1t} - u_{1\mathrm{tP}}; u_{2t} - u_{2\mathrm{tP}}; u_{3t} - u_{3t\mathrm{P}})^{i-1}/\delta n$.

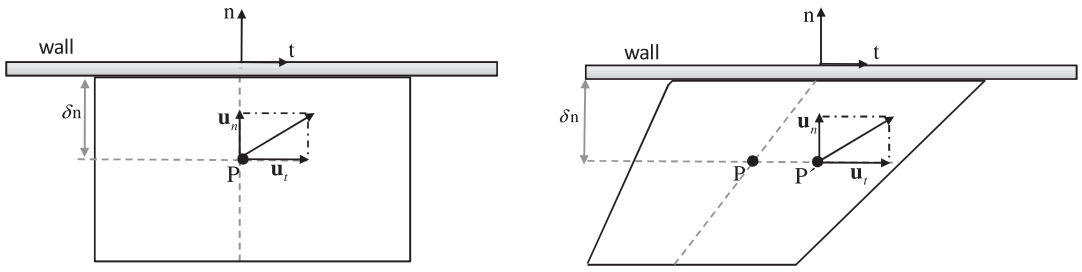

Figure 4. Projection of the velocity vector in the center of the computational cell into the tangent and normal part (left, orthogonal mesh; right, nonorthogonal mesh).

DOI: 10.1002/fld

Notice that $u_{jws} < u_{jtP}$ seems to be sufficient to obtain a stable computation. In our tests, this procedure worked well, except for very high slip coefficients with the Hatzikiriakos law, where convergence was difficult. More details on this issue can be found in the following section.

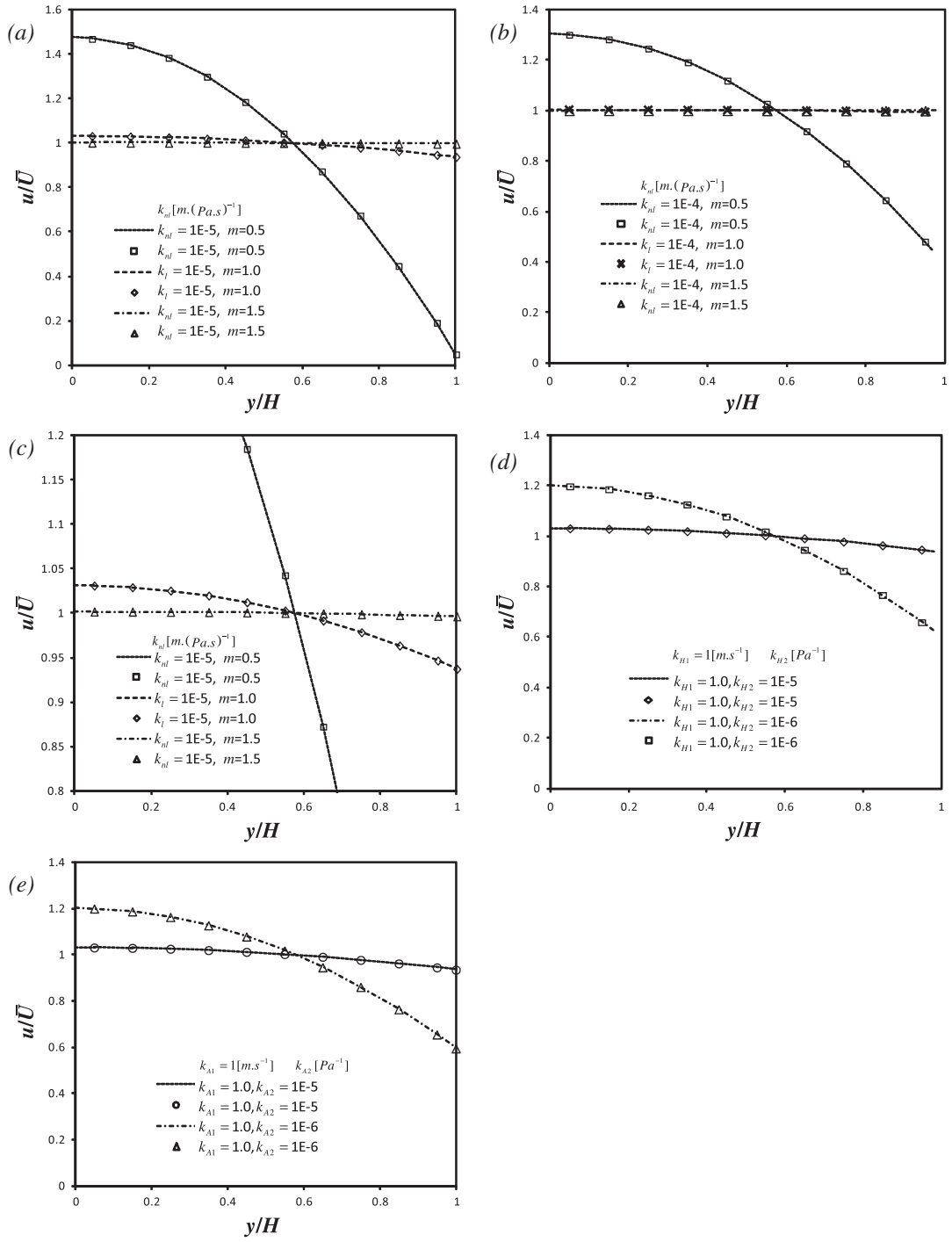

Figure 5. Comparison between analytical (lines) and numerical (symbols) solutions for a fully developed channel flow using linear and nonlinear slip laws with different slip coefficients: (a) nonlinear Navier slip law with $k_{nl} = 1E-5$; (b) nonlinear Navier slip law with $k_{nl} = 1E-4$; (c) zoomed view of the nonlinear Navier slip law with $k_{nl} = 1E-5$; (d) Hatzikiriakos slip law; and (e) asymptotic slip law. $\overline{U}$ is the imposed mean velocity, and H is half the channel width.

DOI: 10.1002/fld

Remark 1

All the previous methods are easy to implement in an iterative procedure. Besides the fully implicit method used for the linear Navier slip model, all other methods in this work are semi-implicit and therefore suffer from stability problems. Another option would involve the explicit inversion of Equations (15)–(17) to express $\frac{\mathrm{d}u}{\mathrm{d}y}$ as a (nonlinear) function of u_{ws}. Such expression could then be substituted into the discretized momentum equation leading to a fully implicit nonlinear formulation. The resulting set of nonlinear equations could then be linearized by means of a Newton algorithm, which generally converges much faster than a Picard iteration. In this way, the boundary condition would become a natural part of the fully nonlinear model, and the problems with monotonicity around the walls would be avoided. It should also be noticed that a semi-implicit advection discretization would enhance the stability of the algorithm. These enhancements would require a huge modification of the original modeling code, thus we adopted a simpler approach that allowed to achieve convergence for the studies performed.

4. RESULTS AND DISCUSSION

To assess the performance of the numerical implementations, the slip models studied here were first compared with analytical solutions for fully developed channel flow with wall slip and subsequently tested for the slip-stick and 4:1 contraction flow problems. The analysis is carried out first for Newtonian fluids and subsequently for viscoelastic fluids.

4.1. Newtonian fluids

Figure 5(a) and (b) compares predictions by the nonlinear Navier slip law (including the particular case of the linear Navier slip law ($m = 1$)) for different values of the model parameters (slip coefficient and exponent) with the corresponding analytical solutions. The comparison between the analytical and numerical solutions for the Hatzikiriakos and asymptotic slip laws can be seen in Figure 5(d) and (e), respectively. The accuracy of the results is quite good as can also be assessed by a zoom of Figure 5(a), shown in Figure 5(c), but more specifically by Figures 6 and 7(a), which plot the relative error in the prediction of the slip velocity as a function of the mesh size for the linear and nonlinear Navier slip laws, respectively. Figure 6 shows that the accuracy and the order of convergence of the solution both increase with the slip coefficient. For instance, for the linear law, the order of convergence increases from 2.14 with $k_l = 10\mathrm{E}{-6}$ [m.(Pa.s)$^{-1}$] to 2.6 for $k_l = 1$

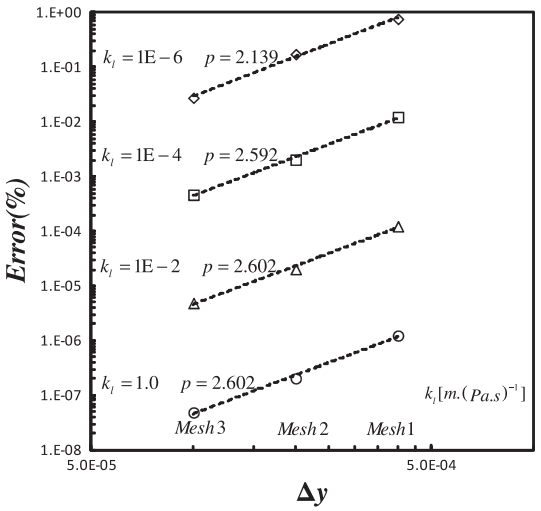

Figure 6. Variation of the relative error in slip velocity with mesh spacing $\triangle y$ for the linear Navier slip law with different slip coefficients and three different meshes ($Re = 0.003$) using the totally implicit scheme (p stands for the order of convergence).

DOI: 10.1002/fld

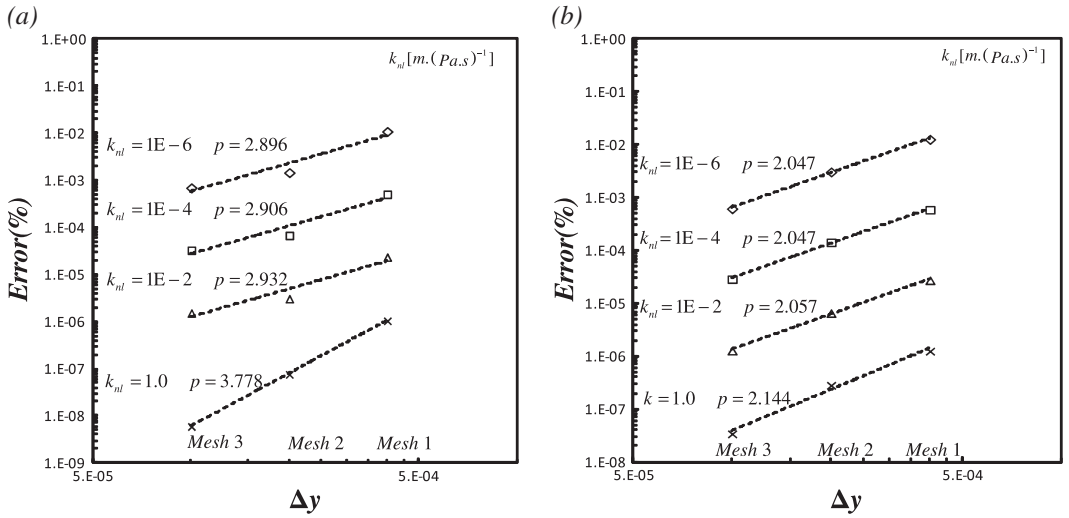

Figure 7. Variation of the relative error in slip velocity with mesh spacing $\triangle y$ for the nonlinear Navier slip law with different slip coefficients and three different meshes ($Re = 0.003$). (a) $n = 1.5$ SSSIT; (b) $n = 1.5$ SSSI. p stands for the order of convergence.

Table I. Uniform meshes used in the channel flow simulations.

	x	y	$\Delta x/H = \Delta y/H$
Mesh 1	25	5	0.2
Mesh 2	50	10	0.1
Mesh 3	100	20	0.05

x stands for the number of cells in the x direction, and y stands for the numbers of cells in the y direction.

[m.(Pa.s)$^{-1}$]. This is so because increasing the slip coefficient leads to higher slip velocities; the velocity profile tends to a plug thus reducing the role of diffusion and increasing that of convection where a third-order accurate scheme [21] is used. Note also that here the error committed in the evaluation of the tangent stress is equal to the error for the slip velocity because the slip velocity depends linearly on the tangent stress $|u_{ws}^{num} - u_{ws}|/|u_{ws}| = |\tau_{12}^{num} - \tau_{12}|/|\tau_{12}|$.

These features are observed regardless of the numerical method used to obtain the solution as can be confirmed in Figure 7(a) and (b), where the order of convergence and error are shown for the predictions obtained with the nonlinear Navier law using the numerical methods SSSIT and SSSI, respectively. Our calculations with the two methods show that the order of convergence increases with the slip coefficient.

Comparing both methods, we found that the order of convergence is larger for the method SSSIT, where at each iteration the 'numerically correct' slip solution is determined by the bisection method, whereas for method SSSI, the solution is only approximated using values from the previous iteration.

After the code assessment, the next step was to compare the various explicit and implicit/semi-implicit schemes using the channel flow of Figure 2 (with the Mesh 2 of Table I), at two different Reynolds numbers of 0.003 and 10 for the four different implementations of slip boundary conditions proposed: (1) totally explicit (SSE), (2) totally implicit (SSI), (3) semi-implicit transcendent (SSSIT) and (4) semi-implicit (SSSI). The linear Navier slip model was chosen for the comparison because all the schemes work with it, and the nonlinear Navier slip model was chosen to compare schemes (3) and (4).

Linear slip model

Figure 8 plots the number of iterations required for convergence and shows that for the implicit procedure (SSI) and this specific geometry and flow, the larger the slip velocity, the quicker is the

DOI: 10.1002/fld

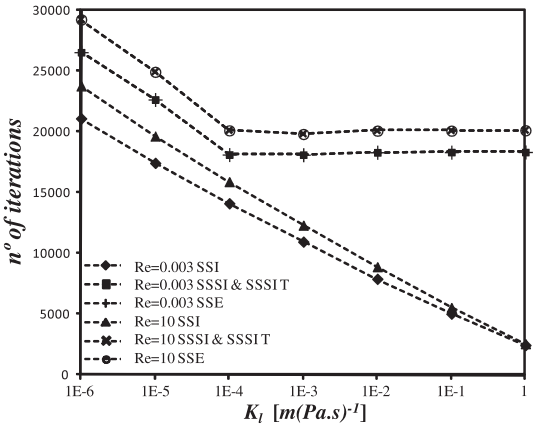

Figure 8. Graph representing a comparison for the number of iterations needed to achieve convergence using the schemes: implicit (SSI), explicit (SSE), semi-implicit transcendent (SSSIT) and semi-implicit SSSI (for the linear Navier slip law) with the simple geometry of Figure 2 (Mesh 2).

convergence. This is so because for large slip, the analytical solution is the plug flow, and the guessed initial velocities are very close to the converged values, so only a few iterations are needed to obtain convergence. For the remaining schemes, similar results were obtained in terms of number of iterations. It should also be noticed that the error for the totally explicit scheme (SSE) was larger than for any other method, because for high slip coefficients the required relaxation factor was sometimes of the same order as the tolerance used to stop the numerical simulation.

From these results, one can conclude that for the linear slip law, the best method is the implicit procedure (SSI).

Nonlinear slip models

The advantages of the semi-implicit procedures (SSSIT and SSSI) can be seen with the nonlinear laws. Table II shows the number of iterations needed to obtain convergence for $Re = 0.003, 10$. The results for the totally explicit method are not shown because convergence was impossible. This results are for a simple geometry, but for a more complex geometry, the capability of the explicit procedure is expected to decrease.

From Table II, it can be seen that for the nonlinear Navier slip law, the number of iterations for methods SSSIT and SSSI was the same. For method SSSI, we found that when $d/(d+1) \approx 1$ (Equation (30)), the code was not able to get out of a periodic sequence where the velocity equals the tangent stress, and to remedy this issue and obtain convergence, a classic relaxation for the slip velocity was used.

For the asymptotic slip law, the schemes SSSIT and SSSI were both efficient, and a similar number of iterations were required for convergence. It should be noticed that when starting the outer iterations, the slip velocity was initialized as 90% of the velocity in the center of the nearest computational cell. Starting with null slip velocity and a constant non-zero velocity at the center of the adjacent computational cells may lead to divergence.

For the Hatzikiriakos slip law, several convergence issues occur, especially for high slip coefficients. For both the SSSIT and SSSI methods, the main problem is due to the hyperbolic function, which either gives very high values at the beginning of the calculations leading to $d/(d+1) \approx 1$ (SSSI) or gives values that cannot be computed by the CPU (SSSIT).

We tried to solve the problem by controlling the growth of the hyperbolic function by limiting the maximum value of the sinh function argument; however, for high velocities, this algorithm does not seem to solve the problem, because convergence could only be obtained for mean velocities below 3 $[\mathrm{m.s}^{-1}]$ ($Re = 0.0091$). The problem seems to be velocity value and not the Reynolds number itself as one could increase the Reynolds number by imposing a mean velocity smaller than 3 $[\mathrm{m.s}^{-1}]$.

DOI: 10.1002/fld

Table II. Number of iterations needed to achieve convergence using the schemes SSSIT and SSSI for the nonlinear Navier slip law with $n = 1.5$, for the Hatzikiriakos and for the asymptotic slip laws.

	Nonlinear NS k_{nl} [m.(Pa.s)$^{-1}$]		Hatzikiriakos $k_{H1} = 1$ [m.s^{-1}] k_{H2} [Pa^{-1}]			Asymptotic $k_{H1} = 1$ [m.s^{-1}] k_{H2} [Pa^{-1}]		
Slip coefficient (k_{nl}, k_{H2})	$Re = 0.003$ SSSIT & SSSI	$Re = 10$ SSSIT & SSSI	$Re = 0.003$ SSSIT	$Re = 0.003$ SSSI	$Re = 10$ SSSIT & SSSI	$Re = 0.003$ SSSIT	$Re = 0.003$ SSSI	$Re = 10$ SSSIT & SSSI
1.0E−06	18,142	19,932	26,398	26,406	Overflow	27,204	27,198	33,049
1.0E−05	17,764	20,049	22,452	22,452	Overflow	23,662	23,663	33,050
1.0E−04	18,266	20,094	Overflow	17,825	Overflow	16,622	19,606	33,048
1.0E−03	18,327	20,111	Overflow	18,165	Overflow	14,944	14,797	33,045
1.0E−02	18,344	20,130	Overflow	18,331	Overflow	13,038	13,331	33,043
1.0E−01	18,348	20,162	Overflow	18,345	Overflow	13,629	13,797	33,042
1.0E+00	18,351	20,157	Overflow	18,354	Overflow	13,680	13,811	33,040

DOI: 10.1002/fld

We also tried to initiate the calculations for the Hatzikiriakos model using the converged results from the linearized version of this model, but convergence was poorly enhanced, and the series expansion of the function did not solve the problem either.

For the Hatzikiriakos slip law, with the scheme SSSIT, only the first two trials converged. So, the chosen method for this slip law is method SSSI, but even here computations are limited to smaller imposed velocities as with higher imposed velocities the sinh function overflows.

4.2. Non-Newtonian fluids

4.2.1. Slip-stick. The simplified PTT model was selected for testing the slip-stick problem in a straight channel (cf. Figure 9) using orthogonal and skewed meshes and the linear and nonlinear slip laws. This flow comprises two regions: the initial part (region I) is unbounded (the upper boundary imposed is a symmetry plane), and the second region (region II) has a solid wall. A symmetry plane was considered at the bottom boundary in both regions. The inlet velocity is a plug profile, and the mesh used has the properties indicated in Table III and Figure 9. The meshes (orthogonal and non-orthogonal) are those of Oliveira *et al.* [10] and correspond to their mesh 7, with a skewness of 30° for the non-orthogonal grid.

Tests were made for different values of the slip coefficients (Table III), at constant Reynolds number $Re = \rho UH/\eta = 20$ and a varying Deborah number $De = \lambda U/H \in \{0.25; 0.5; 1.0; 2.0\}$ with $\varepsilon = 0.25$. Convergence could be achieved for all cases when the mesh was orthogonal and for all the slip laws, whereas for the skewed mesh, convergence was only possible for a Deborah number of up to 2. As expected, an easier convergence could be seen for high slip velocities (high slip coefficients), because the slip velocity numerically smoothes the singularity at the wall.

In Figure 10, one can see the effect of slip in the flow variables u, τ_{xx}, τ_{xy} and τ_{yy} along the line $y/H = 0.9975$ (near the wall). As expected, near the singularity, the variation of all variables tend to smooth with the slip coefficient, and this is especially clear with the stresses that develop because of the extensional nature of the flow in the vicinity of the singularity. As the fluid moves away from the singularity, the stresses start to redevelop for shear flow. As the slip coefficient increases, the slip velocity increases, and the shear rate tends to zero. This reduces the transverse transfer of momentum by molecular diffusion, and flow redevelopment is slowed down. This can be seen especially for the case of τ_{xx} with $k_l = 1\text{E}{-}4$ [m.(Pa.s)$^{-1}$] (Figure 10(b)).

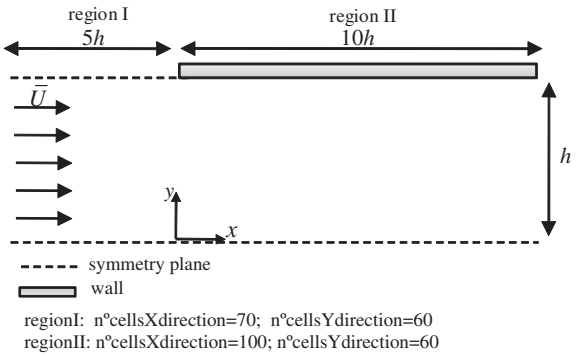

Figure 9. Schematic representation of the slip-stick geometry.

Table III. Slip constants used in the simulation of the slip-stick flow for the different slip models.

Linear Navier	$k_l = 1.0\text{E}{-}a$, $a \in \{1; 2; 3; 4; 5; 6\}$ [m.(Pa.s)$^{-1}$]	
Nonlinear Navier	$k_{nl} \in \{1.0\text{E}{-}5; 1.0\}$ [m.(Pa.s)$^{-1}$]	
Hatzikiriakos	$k_{H1} = 1.0$ [m.s^{-1}]	$k_{H2} \in \{1.0\text{E}{-}5; 1.0\}$[m.s^{-1}]
Asymptotic	$k_{A1} = 1.0$ [Pa^{-1}]	$k_{A2} \in \{1.0\text{E}{-}5; 1.0\}$ [Pa^{-1}]

DOI: 10.1002/fld

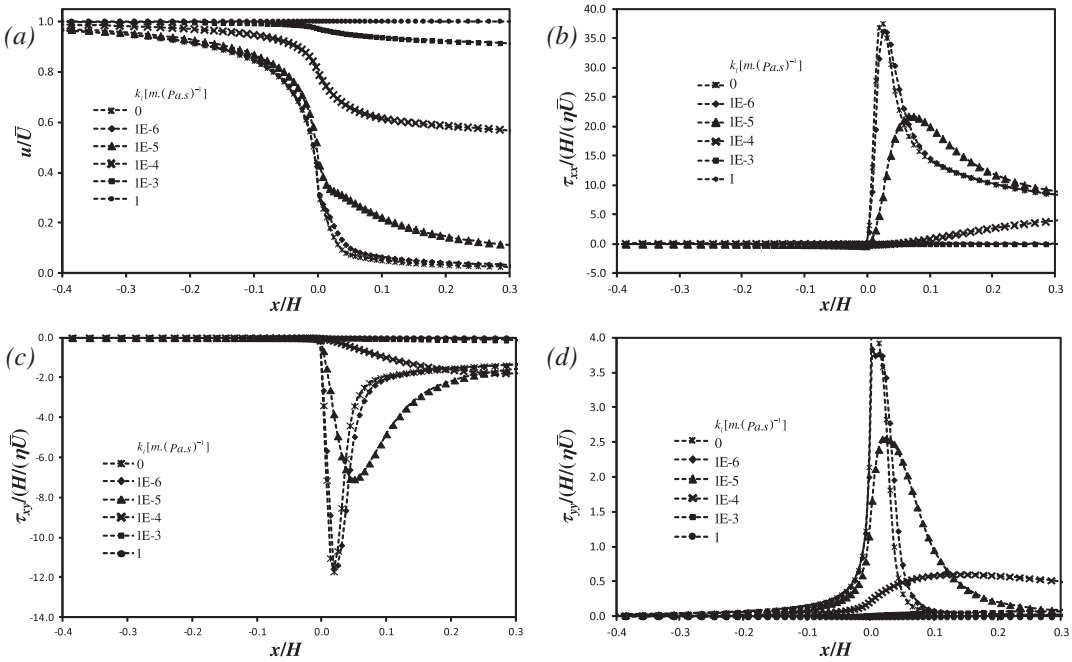

Figure 10. Variation of: (a) u, (b) τ_{xx}, (c) τ_{xy} and (d) τ_{yy} along the slip-stick region near the wall $y/H = 0.9975$. Four different slip constants were used $k_l \in \{1E-6, 1E-5, 1E-4, 1E-3\}$ and $De = 2$, $Re = 20$.

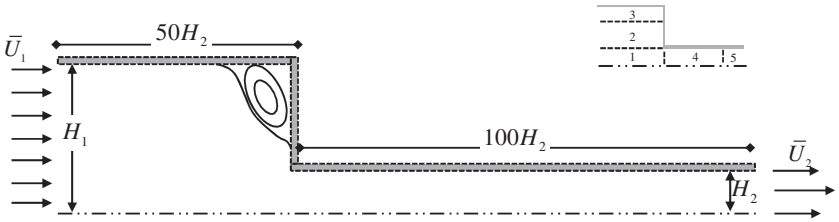

Figure 11. Schematic of the 4:1 contraction geometry.

4.2.2. Contraction flow. The second benchmark flow problem tested for viscoelastic fluids (under the influence of slip) was the planar 4:1 contraction flow.

The geometry for this problem is given in Figure 11 and was divided into five blocks (Table IV) with only half of the channel being considered because of symmetry. On the basis of the work of Oliveira *et al.* [10], Alves *et al.* [22] and Ferrás *et al.* [23], we built three different meshes with consistent mesh refinement between consecutive meshes (MC1, MC2 and MC3 as in Table IV). The notations n_x and n_y are used to represent the number of cells in the x and y directions, respectively, and f_x and f_y are the corresponding contraction/expansion ratios that allow the concentration of cells in zones were high gradients are expected to occur. The most refined mesh (MC3) has almost 200,000 cells.

The simulations were performed for the sPTT model with a constant Reynolds number $Re = \rho U_2 H_2/\eta = 0.04$ and a varying Deborah number $De = \lambda U_2/H_2 \in \{0; 1; 2; 3; 4; 5\}$ with $\varepsilon = 0.25$ and viscosity ratio $\beta = \frac{\eta_s}{\eta_0} = \frac{\eta_s}{\eta_s+\eta_p} = \frac{1}{9}$.

The method that was tested was the SSSI because of its good results in the previous geometries, and the chosen viscoelastic model was again the linear PTT model.

For the linear Navier slip law, we could obtain convergence only up to a De number of 5. As expected, convergence is reduced with the mesh refinement. It should be noticed that for the no-slip

DOI: 10.1002/fld

Table IV. Mesh properties for the 4:1 contraction geometry.

	MC1				MC2				MC3			
Zone	f_x	f_y	n_x	n_y	f_x	f_y	n_x	n_y	f_x	f_y	n_x	n_y
1	0.93500	0.95950	87	36	0.96695	0.97950	174	72	0.98334	0.98972	348	144
2	0.93500	1.04860	87	47	0.96695	1.02400	174	94	0.98334	1.01193	348	188
3	0.93500	0.92700	87	18	0.96695	0.96280	174	36	0.98334	0.98123	348	72
4	1.06952	0.95950	87	36	1.03418	0.97950	174	72	1.01694	0.98972	348	144
5	1.00000	0.95950	15	36	1.00000	0.97950	30	72	1.00000	0.98972	60	144
		nº cells		12459		nº cells		49836		nº cells		19,9344
		Δ min		0.010		Δ min		0.005		Δ min		0.002

DOI: 10.1002/fld

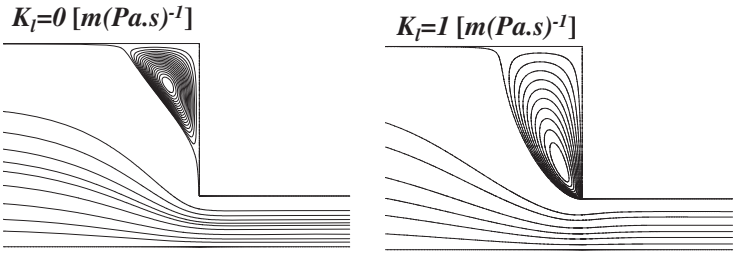

Figure 12. Vortex size for the 4:1 contraction flow of a PTT fluid for two different slip coefficients $k_l = 0$ and $k_l = 1$.

velocity boundary condition, no restrictions were found in the De number for this specific geometry and constitutive equation [22].

On the basis of the results obtained for the linear Navier slip law, it is expectable that the other nonlinear slip laws will again suffer from poor convergence. Because the Hatzikiriakos slip law is the most difficult slip law to compute, we also tested the limits on the De number for the Hatzikiriakos slip law. We could obtain convergence up to $De = 1$ with $k_{H1} = 1$ and $k_{H2} = 1\text{E}{-4}$.

We could also find that the presence of slip velocity leads to an increase of the vortex size (Figure 12; see [23] for more details).

5. CONCLUSIONS

Several new explicit, implicit and semi-implicit numerical techniques were developed to implement slip boundary conditions into a FVM-based code. These implementations are 'stable' for the linear and nonlinear Navier and asymptotic slip laws. However, the Hatzikiriakos slip model leads to unstable behavior for high slip coefficients leading to divergence of the code. Some ad hoc procedures were presented to attenuate this divergence, but these never solved completely the problem that is rooted on the sinh function and the corresponding computer overflow it creates. The predictions given by the numerical code were compared with the analytical solutions, and excellent agreements were obtained for Newtonian fluids. Finally, the implementations were tested with viscoelastic fluids in the slip-stick and planar 4:1 contraction benchmark flows, evidencing the robustness of the proposed numerical procedures.

APPENDIX A: DISCRETIZATION OF THE MOMENTUM EQUATION FOR A SIMPLE 2D GEOMETRY

The continuity and momentum equations can be written in Cartesian coordinates as Equations (A.1) and (A.2), respectively,

$$\frac{\partial u}{\partial x} + \frac{\partial u}{\partial y} = 0 \tag{A.1}$$

$$\frac{\partial(\rho\phi)}{\partial t} + \frac{\partial(u\phi)}{\partial x} + \frac{\partial(v\phi)}{\partial y} = -\frac{\partial p}{\partial \Psi} + \frac{\partial}{\partial x}\left(\eta_s \frac{\partial \phi}{\partial x} + \tau_{\Psi x}\right) + \frac{\partial}{\partial y}\left(\eta_s \frac{\partial \phi}{\partial y} + \tau_{\Psi y}\right) \tag{A.2}$$

where $\phi = u$ and $\Psi = x$ in the x-momentum equation, and $\phi = v$ and $\Psi = y$ in the y-momentum equation. The discretization of the continuity equation in a computational cell P (Figure 2) results in the balance of mass fluxes for this cell. These fluxes are normal to the cell faces; therefore, the slip boundary condition has no direct influence on this equation (because the walls are impermeable). The momentum equation is directly affected by the slip boundary condition, and for that reason, its discretization is briefly explained in the succeeding text. The interested reader should consult [9, 10] for more details.

DOI: 10.1002/fld

In the momentum equation (Equation (A.2)), the discretization of the transient, convective and pressure gradient terms is not directly affected by the implementation of slip velocity, but the diffusive term is affected, as explained next.

The discretization of the *transient* term using a first-order scheme is given by Equation (A.3). The variable ϕ is evaluated at the center of the cell P, meaning that this term is not directly affected by the slip velocity (the superscript '0' indicates the previous time step, and compass notation is used, i.e., *e* stands for 'east', *w* for 'west", *n* for 'north' and *s* for 'south' cell faces).

$$\int_w^e \int_s^n \int_{t_0}^{t_1} \frac{\partial(\rho\phi)}{\partial t} \mathrm{d}t\mathrm{d}x\mathrm{d}y = \int_w^e \int_s^n (\rho\phi) - (\rho\phi)^0 \mathrm{d}x\mathrm{d}y \approx [(\rho\phi)_\mathrm{P} - (\rho\phi)_\mathrm{P}^0]\Delta V_\mathrm{P} \tag{A.3}$$

For the fully implicit method in time used here, all other terms are evaluated at the present time step.

Discretization of the *convective* terms results in Equation (A.4) for the x- and y-momentum equations. Although the variable of interest ϕ_n (cf. Figure 1) appears in Equation (A.4), for impermeable walls, this wall-normal convective term has no contribution from the slip boundary condition ($\mathrm{F}_n = \Delta y \rho v = 0$).

$$\int_w^e \int_s^n \int_{t_0}^{t_1} \frac{\partial(u\phi)}{\partial x} + \frac{\partial(v\phi)}{\partial y} \mathrm{d}t\mathrm{d}x\mathrm{d}y \approx (\mathrm{F}_e\phi_e - \mathrm{F}_w\phi_w)\Delta t + (\mathrm{F}_n\phi_n - \mathrm{F}_s\phi_s)\Delta t \tag{A.4}$$

The discretization of the *diffusive* term for the PTT fluid together with the assumption of Equation (14) leads to the following expression to be incorporated the x- and y-momentum equations:

$$\left[\left(\mu(\dot{\gamma})\frac{\partial\phi}{\partial y}\right)_{n\equiv\mathrm{wall}} - \left(\eta_s\frac{\partial\phi}{\partial y} + \tau_{\Psi y}\right)_s\right]\Delta x\Delta t + \left[\left(\eta_s\frac{\partial\phi}{\partial x} + \tau_{\Psi x}\right)_e - \left(\eta_s\frac{\partial\phi}{\partial x} + \tau_{\Psi x}\right)_w\right]\Delta y\Delta t \tag{A.5}$$

Notice that the terms for the north cell face $(...)_n$ at Equation (A.5) came from Equation (14) (the north cell face is a boundary face). The slip velocity is then carried via $\left(\frac{\partial\phi}{\partial y}\right)_{n\equiv\mathrm{wall}}$. Different one-sided approximations to the derivatives can be used, such as the first-order scheme of Equation (A.6) or the second-order accurate scheme of Equation (A.7). Assuming uniform meshes, the first and second-order approximations are respectively given by

$$\left(\frac{\partial\phi}{\partial y}\right)_{\mathrm{wall}} = \frac{\phi_{\mathrm{wall}} - \phi_\mathrm{P}}{\Delta y_f} + O(\triangle y) \tag{A.6}$$

$$\left(\frac{\partial\phi}{\partial y}\right)_{\mathrm{wall}} = \frac{8\phi_{\mathrm{wall}} - 9\phi_\mathrm{P} + \phi_\mathrm{S}}{6\Delta y_f} + O(\triangle y)^2 \tag{A.7}$$

Assuming square computational cells and the use of central differences to discretize all diffusion-related derivatives (except at the boundaries), the first term in Equation (A.5) becomes Equations (A.8) and (A.9) for the first-order and second-order approximations, respectively,

$$\left[\frac{\mu(\dot{\gamma})_{\mathrm{wall}}}{\Delta y_f}\phi_n + \frac{(\eta_s)_s}{\Delta y}\phi_\mathrm{S} - \left(\frac{\mu(\dot{\gamma})_{\mathrm{wall}}}{\Delta y_f} + \frac{(\eta_s)_s}{\Delta y}\right)\phi_\mathrm{P} + (\tau_{\Psi y})_s\right]\Delta x\Delta t \tag{A.8}$$

$$\left[\frac{8\mu(\dot{\gamma})_{\mathrm{wall}}}{6\Delta y_f}\phi_n + \left(\frac{\mu(\dot{\gamma})_{\mathrm{wall}}}{6\Delta y_f} + \frac{(\eta_s)_s}{\Delta y}\right)\phi_\mathrm{S} - \left(\frac{9\mu(\dot{\gamma})_{\mathrm{wall}}}{\Delta y_f} + \frac{(\eta_s)_s}{\Delta y}\right)\phi_\mathrm{P} + (\tau_{\Psi y})_s\right]\Delta x\Delta t \tag{A.9}$$

After grouping all the terms, the discretized momentum equation is rewritten in the standard compact form (where we have now substituted the general variable ϕ by the specific variable u, because we are analyzing the x-momentum equation)

$$a_\mathrm{P}u_\mathrm{P} = a_\mathrm{E}u_\mathrm{E} + a_\mathrm{W}u_\mathrm{W} + a_\mathrm{S}u_\mathrm{S} + \underbrace{a_\mathrm{N}u_\mathrm{N} + \frac{\Delta V_\mathrm{P}(\rho\phi)_\mathrm{P}^0}{\Delta t} + \frac{\delta p}{\delta\Psi} + S_{\mathrm{stress}}}_{\text{source terms}} \tag{A.10}$$

DOI: 10.1002/fld

where $\frac{\delta p}{\delta \Psi}$ represents a general discretization of the pressure gradient, and a_{E}, a_{S} and a_{W} are given by Equations (A.11), (A.12) and (A.13), respectively,

$$a_{\mathrm{E}} = a_{\mathrm{E}}^c + a_{\mathrm{E}}^d = a_{\mathrm{E}}^c + \frac{(\eta_s)_e \Delta y}{\Delta x} \text{ (first and second order)} \tag{A.11}$$

$$a_{\mathrm{S}} = a_{\mathrm{S}}^c + a_{\mathrm{S}}^d = \begin{cases} a_{\mathrm{S}}^c + \frac{(\eta_s)_s \Delta x}{\Delta y} \text{ (first order)} \\ a_{\mathrm{S}}^c + \left(\frac{\mu(\dot{\gamma})_{\mathrm{wall}}}{6\Delta y_f} + \frac{(\eta_s)_s}{\Delta y} \right) \Delta x \text{ (second order)} \end{cases} \tag{A.12}$$

$$a_{\mathrm{W}} = a_{\mathrm{W}}^c + a_{\mathrm{W}}^d = a_{\mathrm{W}}^c + \frac{(\eta_s)_w \Delta y}{\Delta x} \text{ (first and second order)} \tag{A.13}$$

with the superscripts c and d referring to the convective and diffusive contributions, respectively. To account for the slip boundary condition, which affects $a_{\mathrm{N}} u_{\mathrm{N}}$, the coefficient a_{N} is given by Equations (A.14) and (A.15) for the first-order and second-order accurate discretization schemes, respectively,

$$a_{\mathrm{N}} = \frac{\mu(\dot{\gamma})_{\mathrm{wall}} \Delta x}{\Delta y_f} \tag{A.14}$$

$$a_{\mathrm{N}} = \frac{8\mu(\dot{\gamma})_{\mathrm{wall}} \Delta x}{6\Delta y_f} \tag{A.15}$$

Finally, the central coefficient a_{P} is given as in the standard procedure [9] by

$$a_{\mathrm{P}} = a_{\mathrm{E}} + a_{\mathrm{W}} + a_{\mathrm{S}} + a_{\mathrm{N}} + \alpha \frac{(\eta_s)_n \Delta x}{6\Delta y} + \frac{\Delta V_{\mathrm{P}} \rho_{\mathrm{P}}^0}{\Delta t} \tag{A.16}$$

with $\alpha = 0$ and $\alpha = 1$ for the first-order and second-order approximations, respectively.

APPENDIX B: SECOND-ORDER DISCRETIZATION OF THE LINEAR NAVIER SLIP LAW

The implicit calculation of the second-order accurate linear Navier slip law is given by Equation (B.1)

$$u_{ws}^i = \frac{9k_l \mu(\dot{\gamma})_{\mathrm{wall}}}{6\Delta y_f + 8k_l \mu(\dot{\gamma})_{\mathrm{wall}}} u_{\mathrm{P}}^i - \frac{k_l \mu(\dot{\gamma})_{\mathrm{wall}}}{6\Delta y_f + 8k_l \mu(\dot{\gamma})_{\mathrm{wall}}} u_{\mathrm{S}}^i \tag{B.1}$$

with the restrictions of Equation (B.2)

$$\begin{cases} u_{\mathrm{P}}^i < \frac{k_l \mu(\dot{\gamma})_{\mathrm{wall}}}{k_l \mu(\dot{\gamma})_{\mathrm{wall}} - 6\Delta y_f} u_{\mathrm{S}}^i & \text{if } k_l \mu(\dot{\gamma})_{\mathrm{wall}} - 6\Delta y_f > 0 \\ u_{\mathrm{P}}^i > \frac{k_l \mu(\dot{\gamma})_{\mathrm{wall}}}{k_l \mu(\dot{\gamma})_{\mathrm{wall}} - 6\Delta y_f} u_{\mathrm{S}}^i & \text{if } k_l \mu(\dot{\gamma})_{\mathrm{wall}} - 6\Delta y_f < 0 \end{cases} \tag{B.2}$$

which are imposed by the need to ensure that $u_{ws}^i < u_{\mathrm{P}}^i$. Under these conditions, the momentum equation for the control volume P is

$$a_{\mathrm{P}} u_{\mathrm{P}} = a_{\mathrm{E}} u_{\mathrm{E}} + a_{\mathrm{W}} u_{\mathrm{W}} + a_{\mathrm{S}} u_{\mathrm{S}} + \underbrace{\frac{\Delta V_{\mathrm{P}} (\rho\phi)_{\mathrm{P}}^0}{\Delta t} + \frac{\delta p}{\delta \Psi} + S_{\mathrm{stress}}}_{\text{source terms}} \tag{B.3}$$

with a_{S} given by

$$a_{\mathrm{S}} = a_{\mathrm{S}}^c + \frac{(\eta_s)_s \Delta x}{\Delta y} - \frac{k_l \mu(\dot{\gamma})_{\mathrm{wall}}}{8k_l \mu(\dot{\gamma})_{\mathrm{wall}} + 6\Delta y_f} u_{\mathrm{S}}^i \tag{B.4}$$

DOI: 10.1002/fld

and a_{P} by

$$a_{\mathrm{P}} = a_{\mathrm{E}} + a_{\mathrm{W}} + a_{\mathrm{S}} + a_{\mathrm{N}} - \frac{8k_l\mu(\dot{\gamma})_{\mathrm{wall}}}{8k_l\mu(\dot{\gamma})_{\mathrm{wall}} + 6\Delta y_f} + \frac{\Delta V_{\mathrm{P}}\rho_{\mathrm{P}}^0}{\Delta t} \tag{B.5}$$

Equation (B.4) shows that a_{S} can become negative, therefore violating the requirement for positive coefficients [9] needed to obtain physically realistic solutions, and this is an important limitation. The condition for positive values of a_{S} cannot be given because it depends on several physical parameters that we do not control.

APPENDIX C: EXISTENCE AND UNIQUENESS OF THE DISCRETIZED SLIP VELOCITY

Hatzikiriakos slip law

We postulate that the relationship between u_{ws}^i and u_{P}^{i-1} must be

$$u_{ws}^i = k_{H1}\sinh\left(\frac{k_{H2}\mu(\dot{\gamma})}{\Delta y_f}(u_{\mathrm{P}}^{i-1} - u_{ws}^i)\right) \tag{C.1}$$

with $u_{ws}^i < u_{\mathrm{P}}^{i-1}$ (the physics of the problem requires the slip velocity to be smaller than the velocity at center of the adjacent computational cell) and that u_{ws}^i and u_{P}^{i-1} are both positive or both negative.

Let us assume, without loss of generality, that they are both positive. It must be proved that

$$\exists(u_{ws}^i)^1 : u_{ws}^i = k_{H1}\sinh\left(\frac{k_{H2}\mu(\dot{\gamma})}{\Delta y_f}(u_P^{i-1} - u_{ws}^i)\right) \wedge 0 \leqslant u_{ws}^i \leqslant u_{\mathrm{P}}^{i-1},$$
$$\forall k_{H1},\, k_{H2},\, \mu(\dot{\gamma}),\, u_P^{i-1} \in \mathbb{R}_0^+ \tag{C.2}$$

Proof

Existence. Because $0 \leqslant u_{ws}^i \leqslant u_{\mathrm{P}}^{i-1}$, then $\exists\delta \in \mathbb{R} : 0 \leqslant \delta \leqslant u_{\mathrm{P}}^{i-1}$, in such a way that u_{ws}^i can be written like $u_{ws}^i = u_{\mathrm{P}}^{i-1} - \delta$. The problem can now be stated as

$$\exists(\delta)^1 : \delta + k_{H1}\sinh\left(\frac{k_{H2}\mu(\dot{\gamma})}{\Delta y_f}\delta\right) - u_{\mathrm{P}}^{i-1} = 0 \wedge 0 \leqslant \delta \leqslant u_{\mathrm{P}}^{i-1},\ \forall k_{H1},\, k_{H2},\, \mu(\dot{\gamma}),\, u_P^{i-1} \in \mathbb{R}_0^+ \tag{C.3}$$

Let $f(\delta) = \delta + k_{H1}\sinh\left(\frac{k_{H2}\mu(\dot{\gamma})}{\Delta y_f}\delta\right) - u_{\mathrm{P}}^{i-1}$, because $f(u_{\mathrm{P}}^{i-1})f(0) < 0$ and $f()$ is a real-valued continuous function on the interval $[0;\, u_{\mathrm{P}}^{i-1}]$, the intermediate value theorem implies that $\exists\delta :\ f(\delta) = 0$.

Uniqueness. Rolle theorem states that for a continuous function in some interval $[a;\, b]$, $f : [a;\, b] \to \mathbb{R}$, between two zeros (say x and y) that belong to that interval, there exists a value $\xi \in\,]x;\, y[\, : f'(\xi) = 0$ (if $f'(\xi) \neq 0$, then there could exist at most one zero). Because $f'(\delta) \neq 0\ \forall\delta \in \mathbb{R}$,

$$f'(\delta) = 1 + k_{H1}\cosh\left(\frac{k_{H2}\mu(\dot{\gamma})}{\Delta y_f}\delta\right)\frac{k_{H2}\mu(\dot{\gamma})}{\Delta y_f} > 0 \tag{C.4}$$

Rolle theorem implies that δ is unique. The existence and uniqueness of u_{ws}^i is now proved. □

More can be said about the bottom bound of u_{ws}^i. Because $\sinh\left(\frac{k_{H2}\mu(\dot{\gamma})}{\Delta y_f}(u_{\mathrm{P}}^{i-1} - u_{ws}^i)\right) > \frac{k_{H2}\mu(\dot{\gamma})}{\Delta y_f}(u_{\mathrm{P}}^{i-1} - u_{ws}^i)$, then

$$u_{ws}^i > \frac{k_{H1}k_{H2}\mu(\dot{\gamma})}{k_{H1}k_{H2}\mu(\dot{\gamma}) + \Delta y_f}u_{\mathrm{P}}^{i-1} \tag{C.5}$$

and the initial range for the bisection method is given by

$$\left[\frac{k_{H1}k_{H2}\mu(\dot{\gamma})}{k_{H1}k_{H2}\mu(\dot{\gamma}) + \Delta y_f}u_{\mathrm{P}}^{i-1};\, u_{\mathrm{P}}^{i-1}\right] \tag{C.6}$$

DOI: 10.1002/fld

Asymptotic slip law

As for the Hatzikiriakos slip model, first the intermediate value theorem will be used to prove the existence of the solution, and then, with the Rolle theorem, we will prove its uniqueness.

Consider the function $f(u_{ws}^i)$ given by

$$f(u_{ws}^i) = u_{ws}^i - k_{A1} ln\left(1 + \frac{k_{A2}\mu(\dot{\gamma})}{\Delta y_f}(u_{\mathrm{P}}^{i-1} - u_{ws}^i)\right) \tag{C.7}$$

Because $f(u_{\mathrm{P}}^{i-1})f(0) < 0$ and $f()$ is a real-valued continuous function on the interval $[0;\ u_{\mathrm{P}}^{i-1}]$, the intermediate value theorem implies that $\exists u_{ws}^i :\ f(u_{ws}^i) = 0$.

Because $f'(u_{ws}^i) > 0$ for $u_{ws}^i \in [0;\ u_{\mathrm{P}}^{i-1}]$, by Rolle theorem, the solution is unique.

Using the identity $ln(x) < x\ \forall x \in \mathbb{R}$, it can be seen that,

$$u_{ws}^i < \frac{k_{A1}k_{A2}\mu(\dot{\gamma}) + k_{A1}\Delta y_f}{k_{A1}k_{A2}\mu(\dot{\gamma}) + \Delta y_f} u_{\mathrm{P}}^{i-1} \tag{C.8}$$

The initial range for the bisection method is then given by

$$\begin{cases} [0;\ u_{\mathrm{P}}^{i-1}] \text{ if } k_{A1} > 1 \\ \left[0;\ \frac{k_{A1}k_{A2}\mu(\dot{\gamma}) + k_{A1}\Delta y_f}{k_{A1}k_{A2}\mu(\dot{\gamma}) + \Delta y_f} u_{\mathrm{P}}^{i-1}\right] \text{ if } k_{A1} < 1 \end{cases} \tag{C.9}$$

APPENDIX D: IMPLEMENTATION OF THE NONLINEAR NAVIER SLIP LAW

The discretized form of the nonlinear Navier slip law (Equation (18a)) can be linearized assuming that only the slip velocity of the linear part comes from the actual iteration as

$$u_{ws}^i = k_{nl}\left(\frac{\mu(\dot{\gamma})^{i-1}}{\Delta y_f}\right)^m (u_{\mathrm{P}}^{i-1} - u_{ws}^i)(u_{\mathrm{P}}^{i-1} - u_{ws}^{i-1})^{m-1}$$

This way, we can solve for the slip velocity variable u_{ws}^i and obtain

$$u_{ws}^i = \frac{l}{1+l} u_{\mathrm{P}}^{i-1} \text{ with } l = k_{nl}\left(\frac{\mu(\dot{\gamma})^{i-1}}{\Delta y_f}\right)^m (u_{\mathrm{P}}^{i-1} - u_{ws}^{i-1})^{m-1}.$$

ACKNOWLEDGEMENTS

The authors acknowledge funding from COMPETE/FEDER and Fundação para a Ciência e a Tecnologia (FCT), Portugal, through project PTDC/EME-MFE/113988/2009, and FEDER, via FCT, under the PEst-C/CTM/LA0025/2011 (Strategic Project - LA 25 - 2011-2012). L.L.F. would like to thank FCT for financial support through the scholarship SFRH / BD / 37586 / 2007.

NOMENCLATURE

a_{E} , a_{W} ,a_{N} ,a_{S}	East, west, north and south neighbor coefficients for the discretized momentum equation
a_{F}	Neighbor coefficients for the discretized momentum equation
a_{F}^{τ}	Neighbor coefficients for the discretized constitutive equation
a_{P}	Central coefficient for the discretized momentum equation
a_{P}^{τ}	Central coefficient for the discretized constitutive equation
$f()$	Function used to represent the slip laws
$f_d()$	Function used to represent the discretized form of the slip laws
i	Iteration number
k_l	Slip coefficient for the Navier slip law
k_{nl}	Slip coefficient for the nonlinear Navier slip law
k_{H1}, k_{H2}	First and second slip coefficients for the Hatzikiriakos slip law

DOI: 10.1002/fld

k_{A1}, k_{A2}	First and second slip coefficients for the asymptotic slip law
m	Exponent of the nonlinear Navier slip law
$\mathbf{n} = (n_1, n_2, n_3)$	Normal (to the wall) velocity vector
p	Pressure
$\boldsymbol{S}$	Deformation tensor
$S_{\mathbf{u}}$	Source term for the momentum equation
$S_{\boldsymbol{\tau}}$	Source term for the stress equation
t	Time
tr	Trace of the stress tensor
$\mathbf{u}$	Velocity vector
$\mathbf{u}_{\mathrm{F}}$	Velocity vector at the center of the neighbor cells
$\mathbf{u}_{\mathrm{P}}$	Velocity vector at the center of the control volume
u_{P}^0	Velocity from the previous time step
$\mathbf{u}_t$	Tangent (to the wall) velocity vector
(u_{1t}, u_{2t}, u_{3t})	Components of $\mathbf{u}_t$
u_{ws}	Slip velocity
$(u_{1t\mathrm{P}}; u_{2t\mathrm{P}}; u_{3t\mathrm{P}})$	Components of the tangent (to the wall) velocity vector $\mathbf{u}_{t\mathrm{P}}$ at the center of the control volume P
V_{P}	Cell volume
$\dot{\gamma}$	Shear rate
δn	Distance between the wall and the center of the adjacent control volume
Δt	Time step
Δy_f	Control volume half height
ε	Parameter related to the elongational behavior of the fluid (PTT constitutive equation)
$\eta(.)$	Viscosity function
η_s	Solvent viscosity
η_p	Zero shear polymer viscosity
λ	Relaxation time (PTT constitutive equation)
$\mu(.)_{\mathrm{wall}}$	Viscosity function at the wall
ρ	Density
$\boldsymbol{\tau}$	Stress tensor
$\boldsymbol{\tau}_s$	Solvent stress tensor
$\boldsymbol{\tau}_p$	Polymeric stress tensor
$\boldsymbol{\tau}_{\mathrm{P}}$	Stress variable at the center of the control volume
$\tau_{xx}, \tau_{xy}, \tau_{xz}, \tau_{yz}, \tau_{yy}, \tau_{zz}$	Components of the stress tensor
$\boldsymbol{\tau}_t$	Tangent (to the wall) stress vector
$(\boldsymbol{\tau}_1, \boldsymbol{\tau}_2, \boldsymbol{\tau}_3)$	Component of $\boldsymbol{\tau}_t$

REFERENCES

1. Liakos A. Discretization of the Navier-Stokes equations with slip boundary condition. *Numerical Methods for Partial Differential Equations* 2001; **17**:26–42.
2. Verfürth R. Finite element approximation of incompressible Navier-Stokes equations with slip boundary condition. *Numerische Mathematik* 1987; **50**:697–721.
3. John V. Slip with friction and penetration with resistance boundary conditions for the Navier-Stokes equations-numerical tests and aspects of the implementation. *Journal of Computational and Applied Mathematics* 2002; **147**:287–300.
4. Stokes YM, Carey GF. On generalized penalty approaches for slip, free surface and related boundary conditions in viscous flow simulation. *International Journal of Numerical Methods for Heat and Fluid Flow* 2010; **21**:668–702.
5. Sunarso A, Yamamoto T, Mori N. Numerical simulation of polymeric flow in contraction channels: wall slip and channel size dependent effects. *FLOW DYNAMICS: The Second International Conference on Flow Dynamics. American Institute of Physics Conference Proceedings* 2006; **832**:341–344.
6. Sunarso A, Yamamoto T, Mori N. Numerical analysis of wall slip effects on flow of Newtonian and Non-Newtonian fluids in macro and micro contraction Channels. *Journal of Fluids Engineering - ASME* 2007; **129**:23–31.

DOI: 10.1002/fld

7. Wesson RD, Papanastasiou TC. Flow singularity and slip velocity in plane extrudate swell computations. *Journal of Non-Newtonian Fluid Mechanics* 1988; **26**:277–295.
8. Guermond JL, Minev P, Shen J. An overview of projection methods for incompressible flows. *Computer Methods in Applied Mechanics and Engineering* 2006; **195**:6011–6045.
9. Patankar SV. *Numerical Heat Transfer and Fluid Flow*. Hemisphere: Washington D. C., 1980.
10. Oliveira P, Pinho FT, Pinto GA. Numerical simulation of non-linear elastic flows with a general collocated finite-volume method. *Journal of Non-Newtonian Fluid Mechanics* 1998; **79**:1–43.
11. Phan-Thien N, Tanner RI. A new constitutive equation derived from network theory. *Journal of Non-Newtonian Fluid Mechanics* 1977; **2**:353–365.
12. Phan-Thien N. A nonlinear network viscoelastic model. *Journal of Rheology* 1978; **22**:259–283.
13. Van Doormaal JP, Raithby GD. Enhancements of the SIMPLE method for predicting incompressible fluid flows. *Numerical Heat Transfer* 1984; **7**:147–163.
14. Gaskell PH, Lau AKC. Curvature-compensated convective transport: Smart, a new boundedness preserving transport algorithm. *International Journal for Numerical Methods in Fluids* 1988; **8**:617–641.
15. Navier C. L. M. H. Sur les lois du mouvement des fluids. *Mémoires de l'Académie des sciences de l'Institut de France* 1827; **6**:389–440.
16. Schowalter WR. The behavior of complex fluids at solid boundaries. *Journal of Non-Newtonian Fluid Mechanics* 1988; **29**:25–36.
17. Hatzikiriakos S. A slip model for linear polymers based on adhesive failure. *International Polymer Processing* 1993; **8**:135–142.
18. ANSYS Polyflow manual (implementation of boundary conditions), 2011. ANSYS.
19. Ferrás LL, Nóbrega JM, Pinho FT. Analytical solutions for Newtonian and Inelastic non-Newtonian flows with wall slip. *Journal of Non-Newtonian Fluid Mechanics* 2012; **175-176**:76–88.
20. Azaiez J, Guénette R, Aitkadi A. Numerical simulation of viscoelastic flows through a planar contraction. *Journal of Non-Newtonian Fluid Mechanics* 1996; **62**:253–277.
21. Leonard BP. A stable and accurate convective modeling procedure based on quadratic upstream interpolation. *Computer Methods in Applied Mechanics and Engineering* 1979; **19**:59–98.
22. Alves MA, Oliveira PJ, Pinho FT. Benchmark solutions for the flow of Oldroyd-B and PTT fluids in planar contractions. *Journal of Non-Newtonian Fluid Mechanics* 2003; **110**:45–75.
23. Ferrás LL, Afonso AM, Alves MA, Nóbrega JM, Carneiro OS, Pinho FT. 4:1 Contraction flow of Phan-Thien Tanner fluids with slip boundary conditions. (Submitted to Journal of Non-Newtonian Fluid Mechanics).

DOI: 10.1002/fld